

1 Introduction

Aldolase provides catalysis of the conversion between the hexose 1,6-fructosebisphosphate (1,6FP2) and the two trioses dihydroxy acetone phosphate (DHAP) and glyceraldehyde 3-phosphate (G3P) which is an important reaction within the processes of glycolysis, glucogenesis, and fructose metabolism. In addition to these substrates, aldolase can catalyze the conversion of other phosphorylated sugars including 1-fructose-phosphate (1FP). Depending on the demands of the tissue that contains the aldolase, aldolase's relative recognition of 1FP and 1,6FP2 must be controlled, which may partially account for the fact that humans have three isozymes of aldolase: aldolase A–prominent in muscle tissue, aldolase B–found primarily in the liver, and aldolase C–associated with brain tissue.

The isozymes' Michelis constants (K_m) for the cleavage of 1,6FP2 and 1FP have been characterized. A review of the literature (Kusakabe1994, Motoki1993, Kitajima1990, Doyle1995, Berthiaume1993, Malay2002, Pezza(unpublished)) results in the K_m 's for 1,6FP2 to be $61 \pm 16 \mu\text{M}$, $5 \pm 5 \mu\text{M}$, and $11.9 \pm 1.6 \mu\text{M}$ for human aldolase A, B, and C, respectively. Likewise, the K_m 's for 1FP are $42,000 \pm 25,000 \mu\text{M}$, $2,500 \pm 1,300 \mu\text{M}$, and $17,000 \pm 1,400 \mu\text{M}$ for human aldolase A, B, and C, respectively. Penhoet et al. (Penhoet 1969) also showed that the activity ratio of 1,6FP2 to 1FP was approximately 50, 1, and 10 for the orthologous rabbit aldolase A, B, and C. These results indicate that aldolase overall binds 1,6FP2 stronger than 1FP, that aldolase B has a binding affinity that is approximately a magnitude stronger than aldolase A's, aldolase C binds intermediately between aldolase A and B, and that the preference for 1,6FP2 over 1FP *in vitro* also follows this trend with aldolase B showing little or no preference between the two substrates.

Previous work has noted that the sequences of the three aldolases are all similar having > 70% pairwise sequence identities. Moreover, aldolase A and C have identical residues within the binding site, and aldolase B has only a single residues, Thr38, within the binding site that differs from aldolase A and C, Ser38. All three isozymes presumably have similar catalytic mechanisms, and it is believed that Arg303 in each isozyme, which we investigate within this work, is involved in this mechanism (reference?). This high degree of similarity within these binding sites belies the difference in the isozymes' binding profiles, and the biophysical characteristics that result in these profiles still is a question of ongoing interest.

Our lab has developed a computational tool, FTMap, that can investigate the biophysics of protein interactions (Brenke2009). Through modeling energetically-favorable positions on the protein for a diverse set of very small molecular probes, regions on the protein surface, termed hot spots, where the protein has a high propensity to form energetically-favorable interactions with a partner molecule can be identified. Such hot spots have been experimentally identified using X-ray Crystallography (Allen1996) and Nuclear Magnetic Resonance (Hajduk2005), and such experimental approaches have shown that an effective drug or other strong-binding ligands must form interactions within some of the identified hot spots(Mattos1996,Hajduk2005). While a good theory has not yet been established explaining this correlation, it is reasonable to observe

that solvated proteins' interactions are dominated by short-range interactions. Thus pieces of a bound ligand molecule farther from a hot spot region than this short-range threshold do not significantly interact with the hot spot suggesting that probes of the size of this threshold should effectively capture the important interactions while reducing the complexity of the overall investigation. Using such probes, FTMap-identified hot spots have been shown to be in good agreement with X-ray crystallography-identified hot spots(Brenke2009) as well as known drug molecules (Landon2007,Cheng2009,Hall2012). In this work, we use FTMap to form a hypothesis concerning the biophysical role of the the 45th residue of the three isozymes, and we also use FTMap to investigate the interaction landscape of phosphate containing probes to suggest a binding trajectory for the 1,6FP2 within its ring form.

2 Materials and Methods

2.1 Protein structures

Protein structures were obtained from the Protein Databank (PDB), www.pdb.org. All structures analyzed by FTMap were of human aldolase. Mapping was conducted on unbound structures: 2ald for aldolase A, 1qo5 for aldolase B, and 1xfb for aldolase C. Mapping was also conducted on the K146A mutant aldolase A bound to 1,6FP2, 6ald, to investigate the role of this mutation to the binding site mapping results. Due to the fact that 1xfb is missing 20 amino acids at its C-terminal region and due to the hypothesis that this region is important in affecting the rate-limiting step of aldolase A, alternative forms of 2ald with 20 C-terminal amino acids removed and 1qo5 with 17 C-terminal amino acids removed were mapped. For the conformational study, 2ald chain A was used for the CTR-bound structure of aldolase A, 1qo5 chain B was used for the CTR-less structure of aldolase B, 1qo5 chain M was used for the CTR-bound structure of aldolase B, and 1qo5 chain A was used for the CTR-bound structure of aldolase B that has Phe357 between Arg45 and Arg303. All structures and FTMap results were visualized using PyMol.

2.2 Sugar-phosphate structures

Sugar-phosphate structure were extracted from bound protein structures obtain from the Protein Databank (PDB), www.pdb.org. Two structures, from the aldolase A structure 4ald and aldolase B structure 1fdj, of bound 1,6FP2 were taken from the PDB to represent the bound forms of 1,6FP2. As a result of the fact that there does not exist a structure of human aldolase B bound to 1,6FP2, the 1fdj structure of 1,6FP2 bound to rabbit aldolase B, which has a sequence identity of 97% with human aldolase B, was used to provide an alternative model for the aldolase-bound 1,6FP2. Due to the fact that X-ray results are static while molecules are dynamic *in vivo*, the overlaps of these two bound conformers with the FTMap results using the 16 and 93 probe sets on each of the three aldolases were used to obtain a rough estimate of

the occupancy of these two states in each of the three aldolases (see Table 1). This occupancy was then used in further analysis to obtain an “averaged ” 1,6FP2 structure for each of the aldolases including aldolase C which has no bound structure. The structure for 1,6FP2 from 6ald was also used in our analyses although it was not treated as a biologically relevant binding mode. The reasoning for this decision is discussed in the “Results”. Additionally, the two bound conformation of dihydroxy acetone phosphate (DHAP) from 1ado, a structure of rabbit aldolase A which has 98% sequence identity with human aldolase A, are treated as biologically relevant binding modes for DHAP in human aldolase A.

2.3 Structure alignment

All structures were aligned to the unbound, aldolase A structure, 2ald. Alignment was done on the C_{α} -carbons of the residues identified to be aligned by sequence analysis.

2.4 Probe sets

Two probe sets were used within this investigation (I can provide materials concerning these probe sets if asked). The first probe set, henceforth the standard set, contains 16 probe molecules that were initially chosen due to their use in MSCS (Brenke2009). The seconded probe set, henceforth the expanded set, contains 93 probe molecules and was developed for the purposes of functional-group clustering. We chose these probes to reflect chemical moieties commonly found in fragment screening libraries (Hartshorn2005), and they were chosen by the following two considerations:

1. We chose thirteen functional groups: amide, amine, amidine, carboxylic acid, chloride, alcohol, fluoride, hydroxamic acid, ether, phenyl, sulfonamide, tetrazole, and methyltrifluoride. From 12 of these compounds we formed 6 probes each by attaching, a methyl, ethyl, isopropyl, isobutyl, furan, or phenyl group. To the phenyl functional group we only formed 5 probes by attaching a methyl, isopropyl, isobutyl, furan, or phenyl group. This results in 77 probes with subsets of the probes sharing various functional moieties.
2. We also included additional ring structures since drugs often have ring-like moieties. This included 1-isobutyl furan, piperidine, napthalene, 5 nitrogen containing aromatic ring structures, and 8 nitrogen containing double ring structures. This results in an additional 16 probes that share similar geometry and, in some circumstances, similar chemistry.

The third probe set, known as the phosphate set, follows the construction method of the expanded probe set. Since aldolase binds molecules with multiple phosphates, the placement of phosphate moieties attached to various carbon sources is of interest. Since neither of the other two sets have any phosphate-containing compounds, a proshphate set of 6 molecules was constructed to model such interaction.

2.5 Computational solvent sampling

The premise behind FTMap is that small organic molecules of various shapes and polarity consistently interact within the same vicinities (called hot spots) that contribute large portion of the binding free energy to a protein-molecule interaction (Hajduk2005,Mattos1996). The solvent mapping algorithm in FTMap⁷ is a direct computational analog of the experimental screening technique known as Multiple Solvent Crystal Structures (Allen1996,Mattos1996), and FTMap has two sampling stages followed by two stage of cluster analysis to model this technique. The individual stages are further detailed in Brenke et al. (2009). Computational mapping individually places each of the small molecular probes on a dense grid around the protein, finds favorable positions using empirical free energy functions, and then further minimizes these positions against the rigid probe for further free energy evaluation. For each probe type, the individual probes are then clustered and the clusters are ranked on the basis of the Boltzmann-averaged free energy. Next, consensus clusters are identified as sites in which different probe clusters overlap.

2.6 Clustering

To simulate the favorable location of a single probe, the results for each of the probes from the FTMap results were clustered using the algorithm developed in Brenke et al. (2009). This algorithm results in a Boltzmann-averaged energy score for each cluster representative, and the representatives with the top six scores are used in further analysis.

To simulate the locations where a diverse set of probes congregate, clustering across probe representatives of all types is done. The resulting consensus sites are ranked by the number of different representatives in the cluster and visualized using PyMol.

2.7 Phosphate substructure clustering

To obtain an idea where the phosphates tended to migrate in the FTMap results, the representatives obtained after the initial clustering for the 6 probes containing phosphates were further analyzed. The *CPO*₄ substructure from these probes was extracted, and the clustering algorithm was applied to all the *CPO*₄ substructures. The resulting clusters were ranked by the number of representatives that contributed to the cluster, and the resulting phosphates were visualized with PyMol.

2.8 Phosphate density visualization

The atomic density of the phosphoruses from all probes was placed into a $0.5 \text{ \AA} \times 0.5 \text{ \AA} \times 0.5 \text{ \AA}$ grid. All phosphorus atoms were added to the nearest grid point so that each grid point contained the total number of phosphorus atoms within the $.125 \text{ \AA}^3$ volume. To account for uncertainty in the atomic position as well as to smooth the resulting grid, the grid point was convolved 3 times consecutively with a step function that is $\frac{1}{27}$ for $i, j, k \in (-1, 0, 1)$ and 0 everywhere else. The resulting density was subsequently contoured at the 1 and 3σ levels using the volume representation within PyMol.

2.9 Conformation generation

The steric constraints placed on Arg303 by the different isozymes and Arg45 in aldolase B may be partially responsible for the different biochemical characteristics of these enzymes. To investigate the space into which Arg303 may extend within aldolase A and B and Arg45 in aldolase B, numerous conformations of these arginines were generated (This work was completed by Dmitri Beglov). Using a library of arginine coformations taken from the PDB as a starting point, clusters of conformations of arginine were generated. These conformations were transposed onto aldolase, and each conformation was minimized in the presence of the static enzyme structure. These minimized conformations were then clustered and ranked by energy. This minimization process resulted in the resolution of clashes between the arginine and surrounding residues, and the resulting minimized conformation clusters may be interpreted to represent the region within the protein that Arg303/Arg45 sample while in solution.

3 Results

3.1 General results

Unbound structures of aldolase A, B, and C excluding the C-terminal region (CTR) were mapped for the sake of binding site comparison. For all maps, the top ranked and most of the highest ranked consensus clusters were found to reside in the active site where 1,6FP2 and 1FP are known to bind in aldolase A and B (see Figure 1). While the results were similar, one observations is worth pointing out. The top ranked consensus clusters migrated to relatively the same position in all three aldolases. This consensus cluster primarily overlaps the 1- and 2-carbons of the 1,6FP2 models. In aldolase A and C, this hot spot also extended in a direction essentially perpendicular to these carbons, and additional consensus clusters (A's 3rd ranked consensus cluster and C's 4th and 6th ranked consensus clusters) were also found in this vicinity. This is in stark contrast with the results for aldolase B which has a conspicuous lack of probes in this perpendicular region possibly due to conformational difference of Arg303 among the

isozymes.

3.1.1 The effect of the CTR in aldolase A

It has been suggested that the CTR is involved in removing dihydroxy acetone phosphate (DHAP) from the active site in aldolase A (reference); therefore, we mapped and compared the results of aldolase A with and without its CTR. Two known conformations of DHAP bound to aldolase A are known from the structure 1ado: one binding in a similar position to the known binding of 1,6FP2 from 4ald (green in Figure 7), which we will term the catalytic conformation, and one binding in a similar position to the known binding of 1,6FP2 from the K146A mutant, 6ald (magenta in Figure 7), which we will term the perpendicular conformation. These two conformations of DHAP were then used for orientation and comparison of the results.

One noticeable difference between the resulting maps from Figure 7 is the ranking of the consensus clusters. Specifically, the ranking of the consensus cluster that is primarily in contact with the perpendicular conformation of DHAP is only ranked 3rd when aldolase A does not contain its CTR but is the top ranked cluster when aldolase A does.

To obtain a quantitative measure of this observation, the number of probe atoms within 2 Å of the sugar-portion of these conformations was counted, and the ratio of this number from the perpendicular and catalytic conformations was calculated. For the CTR-less form of aldolase A, this ratio is 1.34, and for the aldolase A with its CTR, this ratio was 1.93. This can be interpreted to mean that the presence of the CTR in aldolase A emphasizes the perpendicular conformation of DHAP thus shifting DHAP away from the catalytic active site. At this point, it is worth noting that the mapping of aldolase C without its CTR has similar consensus clusters in this region to the mapping of aldolase A without its CTR (compare Figures 2(a) and 2(d)); however, aldolase B has no probes near the perpendicular conformation of DHAP (Figure 2(c)) in either of its maps (see Figure 6).

3.1.2 The effect of the CTR in aldolase B

The role of the CTR in aldolase B was also investigated. As can be seen in Figure 6, the presence of aldolase B's CTR brings more probes and consolidates existing probes in the region of the 6-phosphate of 1,6FP2. Supporting the importance of this region, the phosphate from the bound form of rabbit aldolase B with its CTR is found between the top and 3rd ranked consensus cluster of human aldolase B with its CTR.

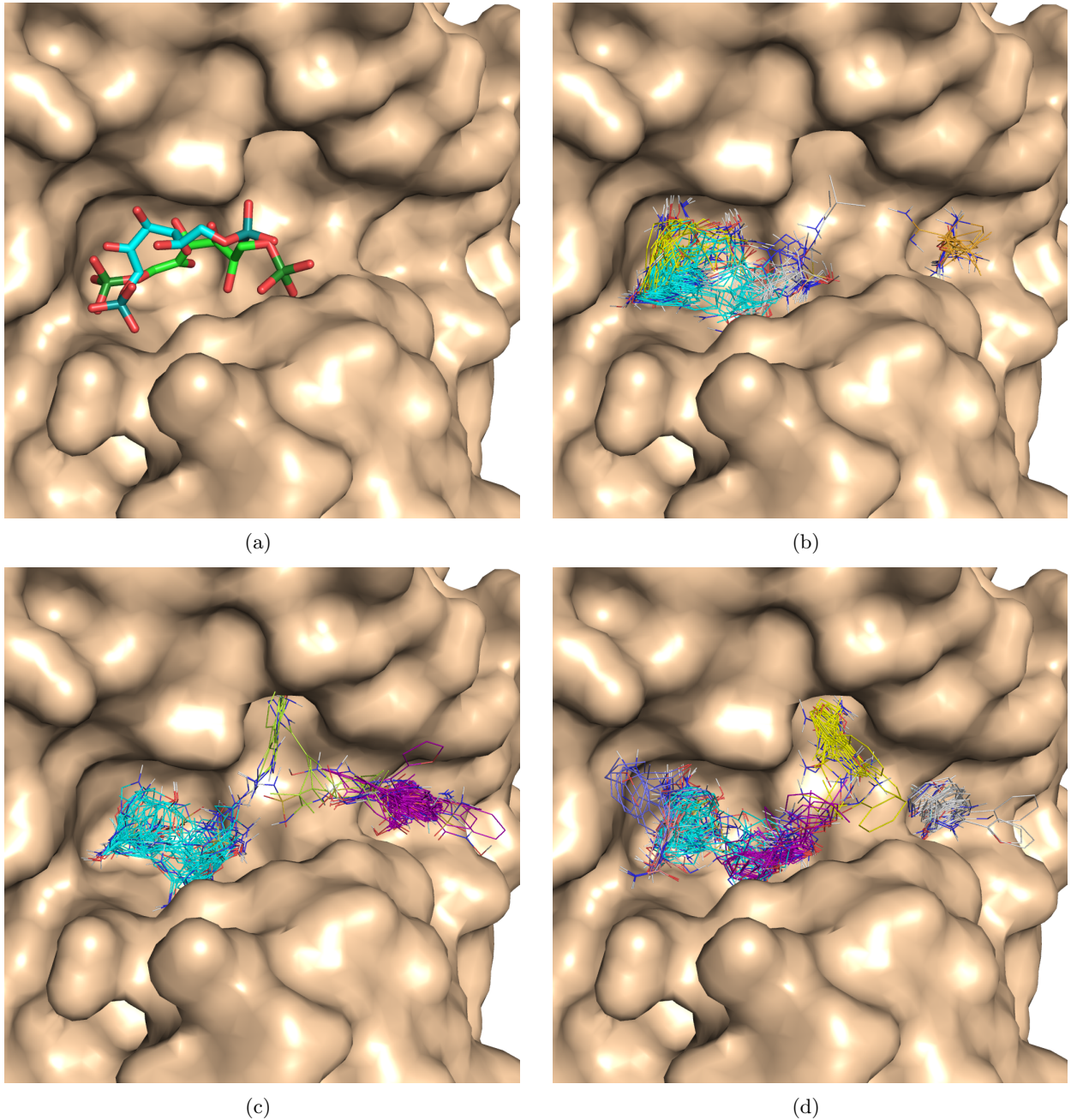


Figure 1: For all parts, the unbound, aldolase A structure without its CTR (cartoon representation colored wheat) was present for the purposes of comparison. (a.) The bound forms of 1,6FP2 from aldolase A (PDB: 4ald) and rabbit aldolase B (PDB: 1fdj). All oxygens of 1,6FP2 are colored red, carbons are colored green and cyan, and phosphates are colored forest green and deep teal for 4ald and 1fdj, respectively. (b.-d.) Consensus rank corresponds to the following coloring scheme: 1 cyan, 2 purple, 3 yellow, 4 salmon, 5 white, 6 periwinkle, 7 orange, 8 green, 9 magenta (b.) The results from mapping unbound, aldolase A without its CTR. (c.) The results from mapping unbound, aldolase B without its CTR. (d.) The results from mapping unbound, aldolase C without its CTR.

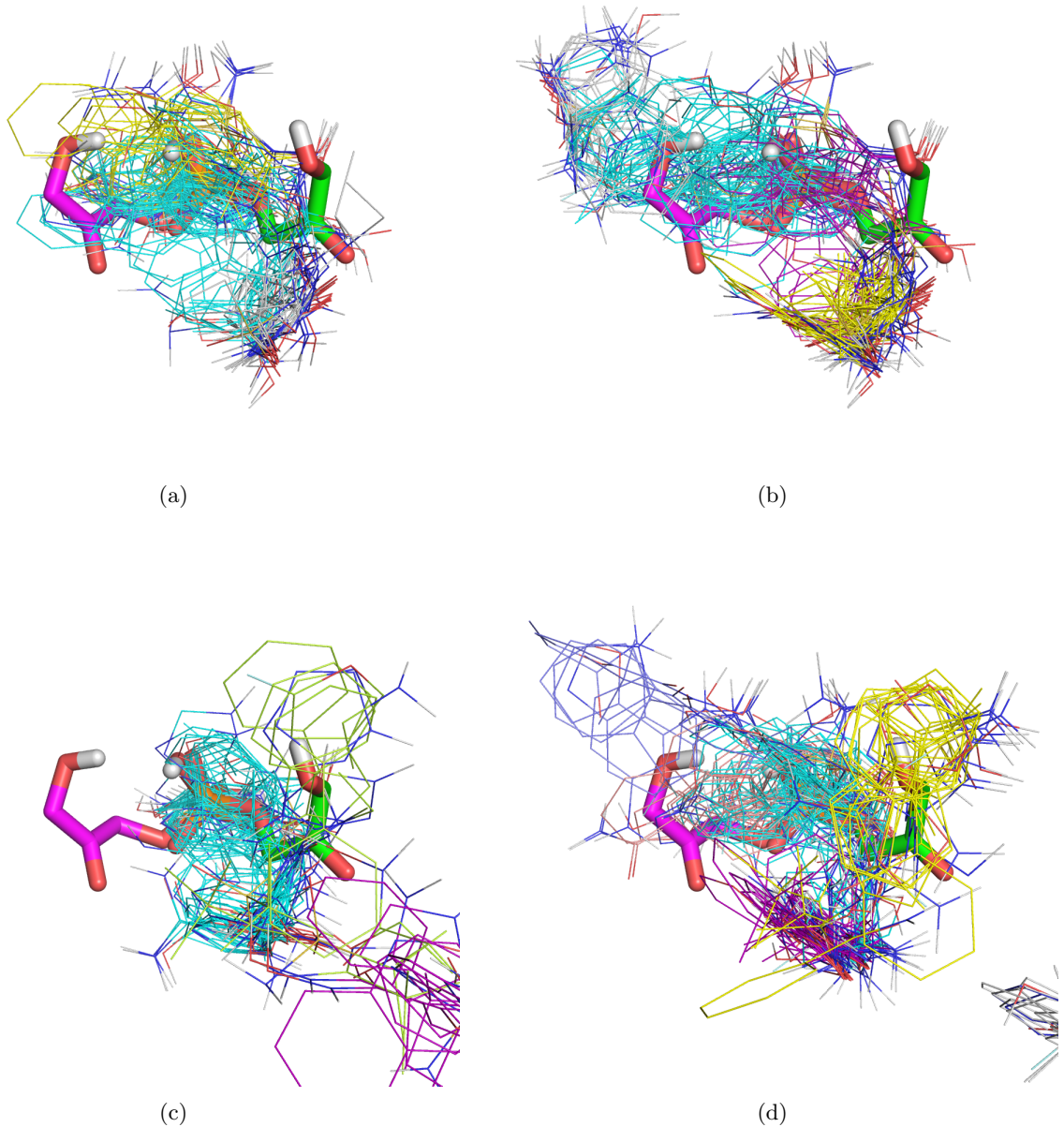


Figure 2: Dihydroxy acetone (DHAP) from the crystal structure of rabbit aldolase A (1aldo) in two conformations (green and magenta). Consensus rank corresponds to the following coloring scheme: 1 cyan, 2 purple, 3 yellow, 4 salmon, 5 white, 6 periwinkle, 7 orange, 8 green (a.) Crossclusters from mapping aldolase A without its CTR superimposed on the DHAP structures. (b.) Crosscluster from mapping aldolase A with its CTR superimposed on the DHAP structures. Notice that the mapping with the CTR has more probes, a different ranking of the crossclusters, and an extension of the top crosscluster in the same direction as the magenta DHAP. (c.) Crossclusters from mapping aldolase B without its CTR superimposed on the DHAP structures. (d.) Crossclusters from mapping aldolase C without its CTR superimposed on the DHAP structures.

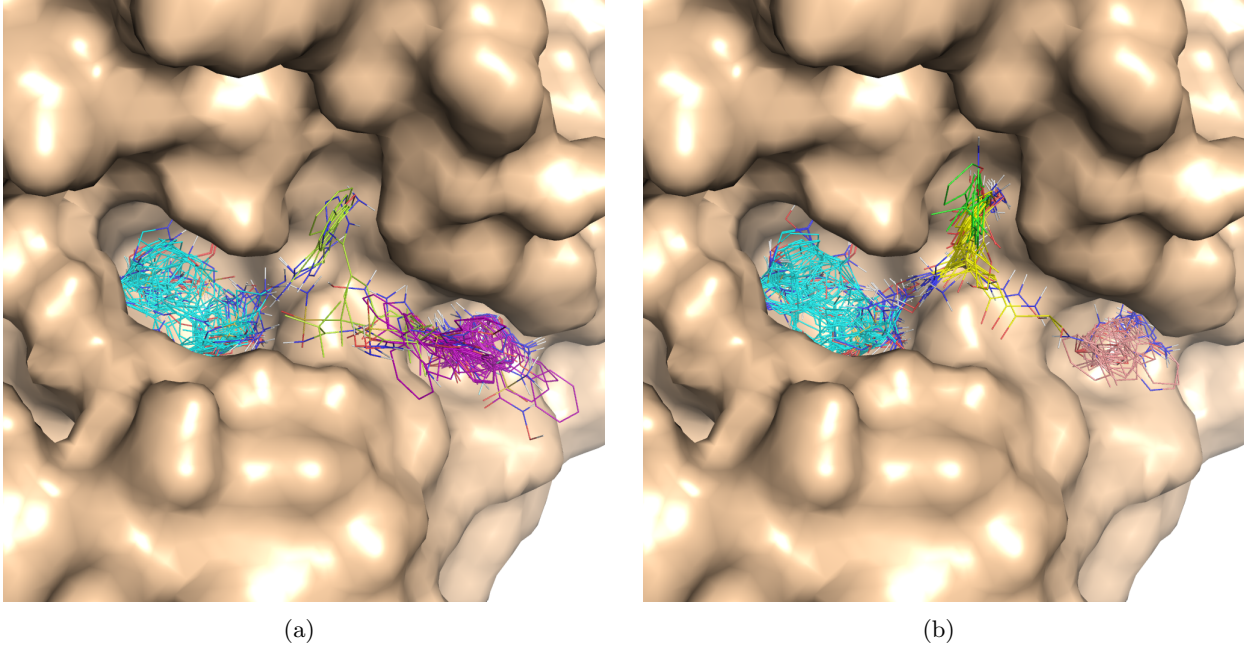


Figure 3: Comparison of mapping results between aldolase B with and without its CTR. Consensus rank corresponds to the following coloring scheme: 1 cyan, 2 purple, 3 yellow, 4 salmon, 5 white, 6 periwinkle, 7 orange, 8 green. The protein structure presented as a wheat surface is that of 1qo5 missing its terminal 17 amino acids (a.k.a. aldolase B without its CTR). (a.) The crossclusters within the active site from the mapping of aldolase B without its CTR. (b.) The crossclusters within the active site from the mapping of aldolase B with its CTR.

3.1.3 Additional consensus regions

In addition to the active site, consistent, significant consensus clusters were found in two other locations. The first additional site is directly next to the active site separated by the loop region consisting of residues 270-276. A consensus cluster was identified in this region in all maps although aldolase B had the largest and highest ranking consensus clusters in this region (ranked 2nd for aldolase B with the CTR). While most residues were conserved across the three isozymes in this region, a number of positions varied (see Table 1). Some differences that may be noteworthy include 235, 245, 248, 274, and 278. These residues point into the cavity towards the consensus clusters, and among the three isozymes, aldolase B always has the smallest of the residues at each position. Another difference that may be noteworthy is the Met274 which is unique to aldolase B. Not only is this residue on the loop that separates the active site from this secondary location, but it is in proximity with Met232 and may be making different interactions with this residue than the glutamines of aldolase A and C.

The second consensus region outside the active site was identified on the opposite end of 2 of

Position	Amino acid		
	A	B	C
191	LEU	LEU	ILE
235	PRO	ALA	PRO
240	THR	THR	PRO
241	GLN	LYS	ILE
243	PHE	TYR	TYR
244	SER	THR	THR
245	HIS	PRO	PRO
274	GLN	MET	GLN
278	GLU	ASP	GLU
281	ILE	LEU	PHE

Table 1: Differences in the neighboring site identified by FTMap. Only residues conserved in all 10 sequences obtained from Uniprot for aldolase B are presented.

Position	Amino acid		
	A	B	C
20	HIS	GLN	LEU
262	PRO	ALA	PRO
265	THR	PRO	PRO
293	LYS	LYS	ARG
296	ALA	LYS	ALA
338	CYS	ALA	ALA

Table 2: Differences in the back site identified by FTMap. Only residues conserved in all 10 sequences obtained from Uniprot for aldolase A are presented. Of special interest is residue 296.

the beta strands which form the beta barrel and which contribute many of the residues which interact with the substrates. As with the other additional site, all maps had a consensus cluster within this region, but aldolase A had multiple and high ranking consensus clusters here (ranked 2nd and 6th for aldolase A without the CTR). Again, most residues are the same among the three isozymes, but there are a number of residues that do vary (see Table 2) which may account for the FTMap result differences. Of specific note is position 296 which is alanine in aldolase A and C but lysine in aldolase B. This residue sits between the two consensus clusters identified in aldolase A without the CTR and therefore significantly occludes this cavity in aldolase B.

3.2 Phosphate mapping

To further investigate the role of the phosphates within the binding of the 1FP and 1,6FP2 by the different isozymes, phosphate probes were used to map the three isozymes. To localize the predicted positions of the phosphates, functional-group clustering was conducted on the six probes containing CPO_4 therefore isolating this chemical moiety. The top 2 phosphate clusters for each isozyme are shown in Figure 5. As can be seen in Figures 4(c) and ??, the phosphates are best localized near the 1P and 6P phosphates of wild-type 1,6FP2 for aldolase A when the CTR is present and are more diffuse when the CTR is removed. For aldolase B (Figure ?? and 4(e)), the 1P site is not present in either map, and the top two sites for the open structure extend towards both wild-type and mutant 6P positions while only the wild-type 6P is identified when the CTR is present in aldolase B. A similar result for the clusters generated by mapping the open aldolase C structure to that of the open aldolase B structure can also be seen in Figure 4(f).

These results suggest that both 6P sites may be present and biologically relevant when the C-terminal region is in its open conformation. Since both of these sites are toward the mouth of the binding site versus the fact that the 1P binding site is deep within the pocket and since these sites are closer together than either site and the 1P site, it may be the case that the ring structure first binds its two phosphates at both of these sites, and that the 1P site is only used once the ring has been opened. To further explore the feasibility of this hypothesis, a phosphorus density from each of the mapping results of the various forms of the three isozymes was created and visualized. As can be seen in Figure ??, the densities of phosphorus atoms seem to trace out two pathways connecting the two 6P phosphate sites to the 1P phosphate site. Consistently, when the structure is open, these pathways extend fully to both 6Ps; however, when the CTR closes upon the site, the phosphate site identified by the 6P from the mutant-1,2FP2 bound structure disappears. This observation supports the interpretation both sites are viable when the CTR is open and further suggests that the phosphate bound within the mutant 6P binding region moves during the closing of the CTR.

3.3 Conformations of Arg303

The differences within the aldolase A, B, and C mapping results near the 1-phosphate binding location suggest different roles for Arg303 within these isozymes. As can be seen by Figure 6(a), the alternative form of Arg303 found within aldolase B overlaps with the perpendicular configuration of DHAP observed in DHAP-bound aldolase A. The aldolase B conformation of Arg303 apparently narrows down this portion of the binding site, and it may largely be responsible for the different behaviors of the two isozymes. Examination of the residues outside of the binding site exposes that Arg45 of aldolase B overlaps with the conformation of Arg303 found within aldolase A and C (see Figure ??). Furthermore, position 45 is differentially conserved among different species as serine in aldolase A and as glutamine in aldolase C suggesting that this residue may be important for differentiating the function of these three isozymes (Tolan's

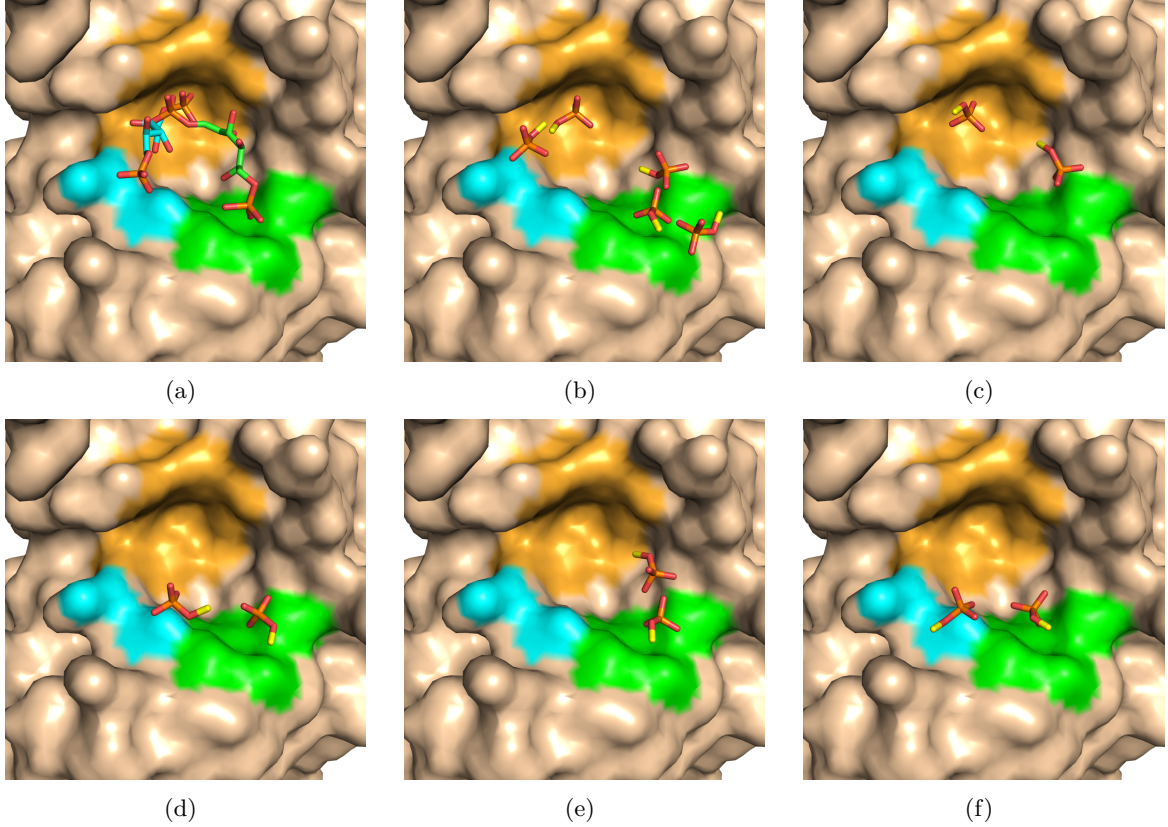


Figure 4: Top two phosphate clusters for various mapping results for the three different isozymes. (a.) A portion of the binding pocket of aldolase A (many aldolase residues have been removed to see into the pocket) overlayed with bound 1,6FP2 from wild-type structure 4ald (green carbons) and mutant structure 6ald (cyan carbons) for reference. Aldolase A represented as wheat unless it is within 6 Å of a phosphate. If the surface is within 6 Å of the common phosphate (1P), it is colored orange, if it is near the 6P of the wild-type 4ald structure, it is colored green, and if it is near the 6P of the mutant 6ald structure it is colored cyan. (b.) The top "two" phosphate clusters for aldolase A without its CTR. Five clusters are tied for the second-ranked position. (c.) The top two phosphate clusters for aldolase A with its CTR. The top two phosphate clusters for aldolase B (d.) without and (e.) with its CTR. The top two phosphate clusters for aldolase C without its CTR.

previous PhD reference). In multiple structures of aldolase B, Arg45 adopts the same conformation regardless of the presence or absence of a tails, therefore, we hypothesize that Arg45 always restricts the conformational space of Arg303.

Furthermore, the CTR in both aldolase A and aldolase B has Phe357; however, one structure of aldolase B has Phe357 within a region that is between Arg45 and Arg303. It is not apparent whether Arg45 is necessary to stabilize the restrictive conformation of Phe357 or whether

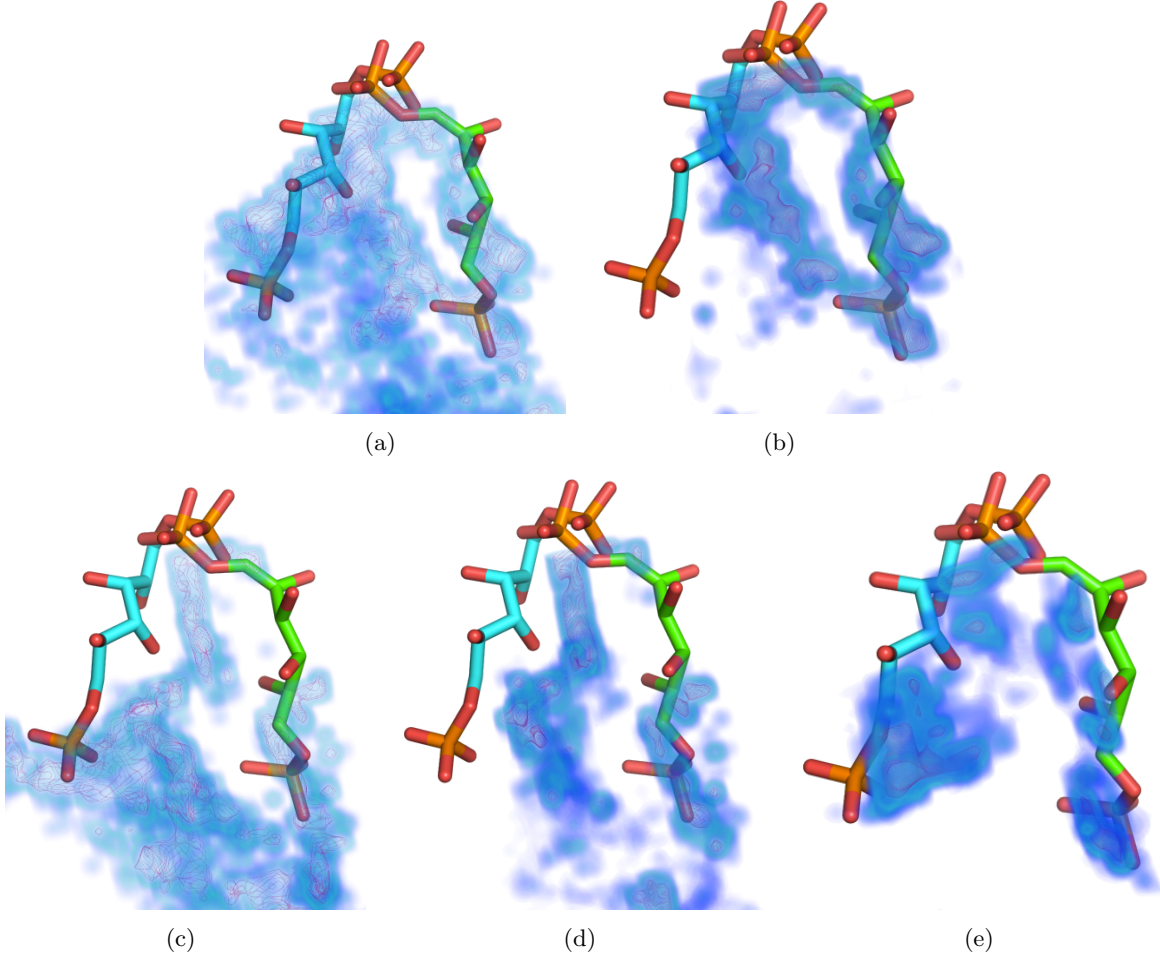


Figure 5: Densities of phosphorus atoms produced by mapping with phosphate probes. The densities are contoured at the 1 (cyan) and 3σ (red) levels, and colored blue between the 0 and 1σ levels. 1,6FP2 from the wild-type 4ald (green carbons) and mutant 6ald (cyan carbons) structures are shown for comparison (a.) A (a.) without and (b.) with its CTR. B (c.) without and (d.) with its CTR. (e.) C without its CTR.

Phe357 from aldolase A may also occupy this conformation but was absent from crystal structures of aldolase A due to crystallization issues, so this difference in Phe357 placement may or may not be associated with the differences in biochemical activity between aldolase A and aldolase B. Regardless, Phe357 is part of the CTR and can only be placed next to Arg303 when the tail conformation is closed, thus the placement of this residue within this region may be part of the function of the tail (at least in B), i.e. the placement of Phe357 may be important in regulating Arg303 as well.

To computationally study the roles of Arg45 and Phe357 in restricting the conformational space of Arg303, conformations of Arg303 were generated for conformation of aldolase A with its

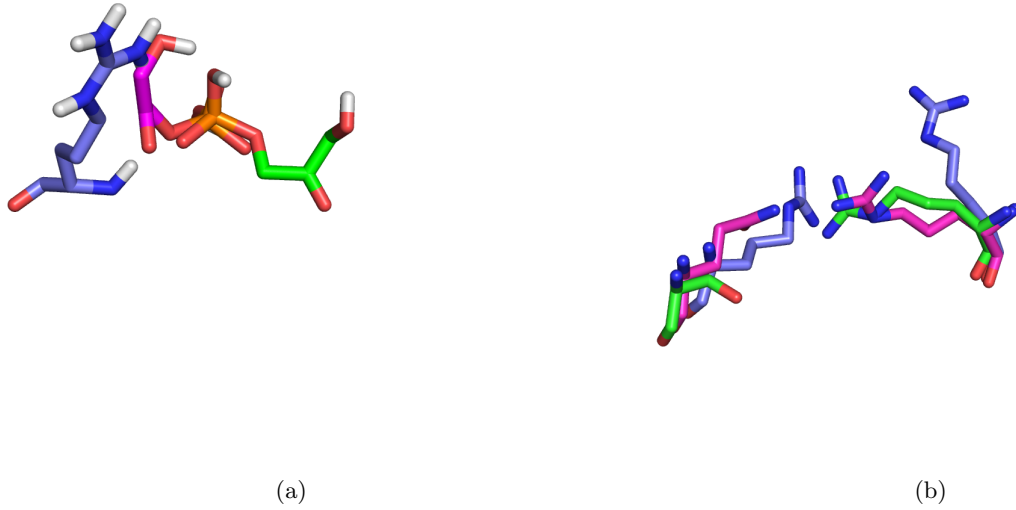


Figure 6: (a.) Two conformations of DHAP (green and magenta carbons) bound to aldolase A taken from 1ado superimposed upon the conformation of Arg303 (slate carbons) found in aldolase B. (b.) Position 45 and 303 for aldolase A (green carbons), aldolase B (slate carbons), and aldolase C (magenta carbons). Position 303 is arginine in all three isozymes, although the conformation of Arg303 is drastically different in B than in A and C. Position 45 is serine in aldolase A, arginine in aldolase B, and glutamine in aldolase C. Notice that Arg45 would clash with Arg303 in aldolase B if Arg303 adopted the conformation seen in aldolase A or C.

CTR and different conformations of aldolase B (see Figure ??). As can be seen in Figures 7(a) and 7(b), while the top conformation energies of Arg303 from the CTR-bound conformation of Adolase A tend to cluster around the actual bound conformation of Arg303, there is also a large confromational region for Arg303 to sample. The conformation of aldolase B with the CTR has a similar region that is slightly restricted by the presence of Arg45 (see Figure 7(c)). This region is further restricted by modeling aldolase B with the CTR that has Phe357 in a similar location to that found in the crystal structure of aldolase A. When the model of aldolase B that has Phe357 placed between Arg45 and Arg303 is used, a highly constricted conformational space for Arg303 that corresponds to the bound form of Arg303 in aldolase B is found 7(d). This suggests that both the presence of Arg45 and Phe357 are important in determining the space within which Arg303 is free to move. If this biophysical observation is important for the biochemical functionality of aldolase B, obtaining R45S of aldolase B should result in similar catalytic behavior for this mutant as is seen in aldolase A. Also, it would be interesting to see if F357A may have a somewhat milder effect on the catalytic behavior of aldolase B. Of course, this would need to be compared to a similar mutant in aldolase A.

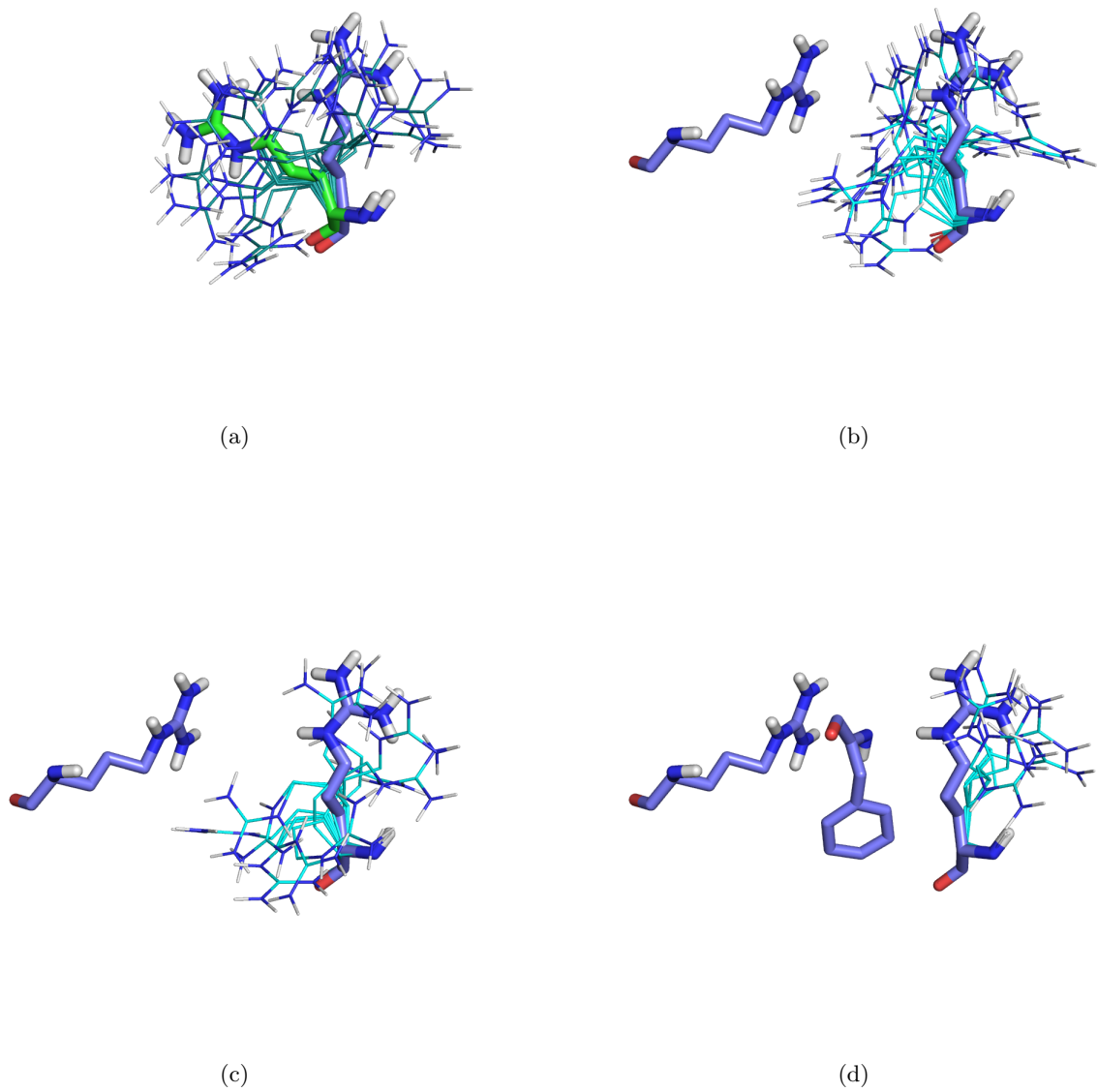


Figure 7: Modelled conformations of Arg303 in various structures of aldolase. (a.) Aldolase A with its CTR. The bound conformation of Arg303 from aldolase A is shown as green sticks, the bound conformation of Arg303 from aldolase B is shown as slate sticks, and the modeled coformations of Arg303 from Adolase A with its CTR are shown as forest green lines. (b.) Aldolase B with no CTR. The bound conformation of Arg303 and Arg45 are shown as slate sticks, and the modelled conformations of Arg303 are shown as cyan lines. (c.) Aldolase B with a conformation of its CTR similar to that of aldolase A. The bound conformation of Arg303 and Arg45 are shown as slate sticks, and the modelled conformations of Arg303 are shown as cyan lines. (d.) Aldolase B with a conformation of its CTR that places Phe357 between Arg303 and Arg45. The bound conformation of Arg303, Arg45, and Phe357 are shown as slate sticks, and the modelled conformations of Arg303 are shown as cyan lines.

4 Conclusions